

Mass function of stellar black holes as revealed by the LIGO-Virgo-KAGRA observations

XIAO-FEI DONG,<sup>1</sup> YONG-FENG HUANG,<sup>1,2,\*</sup> ZHI-BIN ZHANG,<sup>3</sup> XIU-JUAN LI,<sup>4</sup> ZE-CHENG ZOU,<sup>1</sup>  
CHEN-RAN HU,<sup>1</sup> CHEN DENG,<sup>1</sup> AND YANG LIU<sup>3</sup>

<sup>1</sup>*School of Astronomy and Space Science, Nanjing University, Nanjing 210023, China*

<sup>2</sup>*Key Laboratory of Modern Astronomy and Astrophysics (Nanjing University), Ministry of Education, Nanjing 210023, China*

<sup>3</sup>*School of Physics and Engineering, Qufu Normal University, Qufu 273165, China*

<sup>4</sup>*School of Cyber Science and Engineering, Qufu Normal University, Qufu 273165, China*

ABSTRACT

Ninety gravitational wave events have been detected by the LIGO-Virgo-KAGRA network and are released in the Gravitational-Wave Transient Catalog. Among these events, 83 cases are definitely binary black hole mergers since the masses of all the objects involved significantly exceed the upper limit of neutron stars. The black holes in these merger events naturally form two interesting samples, a pre-merger sample that includes all the black holes before the mergers and a post-merger sample that consists of the black holes generated during the merging processes. The former represents black holes that once existed in the Universe, while the latter represents newly born black holes. Here we present a statistical analysis on these two samples. The non-parametric  $\tau$  statistic method is adopted to correct for the observational selection effect. The Lynden-Bell's  $C^-$  method is further applied to derive the mass distribution and density function of black holes. It is found that the mass distribution can be expressed as a broken power-law function. More interestingly, the power-law index in the high mass region is comparable for the two samples. The number density of black holes is found to depend on redshift as  $\rho(z) \propto z^{-2.06} - z^{-2.12}$  based on the two samples. Implications of these findings on the origin of black holes are discussed.

*Keywords:* Black holes (162); Astronomy data analysis (1858); Stellar mergers (2157); Gravitational waves (678)

1. INTRODUCTION

As the first gravitational wave (GW) event being detected, GW150914 was produced by the merger of two black holes (BHs) whose masses are  $m_1 = 36_{-4}^{+5}M_\odot$  and  $m_2 = 29_{-4}^{+4}M_\odot$ , respectively (Abbott et al. 2016a). Since then, the LIGO-Virgo-KAGRA (LVK) gravitational wave detector network (LIGO Scientific Col-

laboration et al. 2015; Acernese et al. 2015; Akutsu et al. 2018) has recorded about 90 confident binary merger events, which are reported in the Gravitational-Wave Transient Catalog (GWTC) <sup>1</sup> (Abbott et al. 2021a, 2023a,b). While the possibility that neutron stars might be involved in four or five GW events still cannot be completely expelled, it is believed that

\* Email:hyf@nju.edu.cn

<sup>1</sup> <https://gwosc.org/>

the majority of the GW events were produced by binary black hole (BBH) mergers. In fact, among the 90 GW events, at least 83 candidates come from BBH systems with the black hole mass ranging in  $5 - 140 M_{\odot}$  (Chattopadhyay et al. 2023; Abbott et al. 2023b). These GW events thus provide a valuable sample of stellar mass black holes.

GW observations provide useful information on the masses and distances of the black hole members, which can be used to probe the binary origin. There are many opinions on the origin of binary black holes, such as binaries in the field area of galaxies with a relatively low stellar density (Bethe & Brown 1998; Giacobbo & Mapelli 2018; Gallegos-Garcia et al. 2021; Abac et al. 2024a), dynamically-driven BBHs in dense stellar clusters (Kulkarni et al. 1993; Portegies Zwart & McMillan 2000; Banerjee et al. 2010; Rodriguez et al. 2016; Chattopadhyay et al. 2022), BBHs originated from triple systems (Antonini et al. 2017; Martinez et al. 2020; Vigna-Gómez et al. 2021), gas capture in the disks of active galactic nuclei (McKernan et al. 2012; Bartos et al. 2017; Fragione et al. 2019; Tagawa et al. 2020). BBHs might also originate as part of a primordial BH population in the early universe (Carr & Hawking 1974; Bird et al. 2016; Ali-Haïmoud et al. 2017; Wu 2020; Ng et al. 2022; Chen et al. 2023). The exact processes that give birth to the BBHs detected by LVK have not yet been conclusively determined (Fakhry 2024), but note that different channels could lead to different BBH characteristics, such as their distributions in mass, spin, distance and other parameters.

Many researchers have tried to infer the physics of binary mergers and the origins of BBHs by studying the distributions of BBH parameters. The parametric method, such as the Bayesian analysis, has been widely applied to a population of BBHs to get the distribution of their physical parameters (population-

level, Foreman-Mackey et al. 2014; Abbott et al. 2016b; Farr et al. 2017; Fishbach et al. 2018; Palmese et al. 2021; Saini et al. 2024). The parameters of a certain BBH can even be inferred in some cases by using this method (event-level, Mandel et al. 2017; Fishbach et al. 2020; Gong et al. 2022; Essick & Fishbach 2024; Rauf et al. 2024). Another popular method is the non-parametric model which does not rely on any pre-assumptions of the parameter distributions (Mandel et al. 2019; Sadiq et al. 2022; Edelman et al. 2023; Callister & Farr 2024; Heinzl et al. 2024). For example, Fishbach et al. (2020) used both parametric and non-parametric method to derive the mass-weighted BBH event rate. It is found that, in contrast to the cut-off feature in the result of the parametric model, the non-parametric model tends to extrapolate smoothly to high masses and provides a conservative upper limit on the rate of high-mass mergers. A semi-parametric method that incorporates a simple parametric component with an additional non-parametric component is also applied to obtain the distribution of BBH parameters (Edelman et al. 2022; Farah et al. 2023; Li et al. 2024b). It explains most of the structure through parametric models while retaining the flexibility of the non-parametric part.

The number of BHs existed in a unit comoving volume, i.e., the comoving BH number density, can provide information on the number of BHs formed at a certain redshift and can help to understand the progenitors of BHs at various stages of evolution (Lloyd-Ronning et al. 2002). However, there are several selection effects in the GW observations of BBHs (Farr 2019; Essick & Fishbach 2024), which prevent us from deriving the redshift distribution and mass distribution of BHs directly. As a result, the number densities of BHs in BBH systems could be derived only when the selection effects are properly accounted for.

The Lynden-Bell’s  $C^-$  method (Lynden-Bell 1971) is usually used to solve mutually independent truncated bivariate data distributions. It has been applied in many fields of astronomy, such as short/long gamma-ray bursts (Lloyd-Ronning et al. 2002; Yu et al. 2015; Pescalli et al. 2016; Zhang & Wang 2018; Liu et al. 2021; Dong et al. 2022, 2023; Li et al. 2024a), fast radio bursts (Deng et al. 2019), galaxies (Kirshner et al. 1978; Loh & Spillar 1986; Peterson et al. 1986) and quasars (Singal et al. 2011; Zeng et al. 2021). The method is quite useful in deriving the intrinsic luminosity functions of various objects based on their flux and redshift measurements. Interestingly, it is also proved to be effective in correcting for the observational selection effects whenever a bivariate (or, more generally, multivariate) distribution is involved (Lynden-Bell 1971; Efron & Petrosian 1992, 1999; Dainotti et al. 2015; Levine et al. 2022).

A key assumption in the  $C^-$  method is about the data independence. Therefore, it is important to ensure the independence of the truncated data. The  $\tau$  statistic method is a unique non-parametric technique widely applied to truncated data for assessing the independence of parameters Efron & Petrosian (1992). The joint operation of the  $\tau$  statistic method and Lynden-Bell’s  $C^-$  method provides an ideal non-parametric method. It is extremely effective for a truncated sample since it does not depend on any pre-assumed models and can give a point-by-point description of the cumulative distribution.

In this study, we adopt the non-parametric method to explore the mass function and redshift distribution of BHs associated with BBH mergers. The BH number density will also be derived based on the analysis. The structure of our paper is organized as follows. In Section 2, data acquisition and the two BH samples used for the analysis are described. Section 3 introduces the non-parametric method and the

calculation processes in detail. The numerical results are presented in Section 4. Finally, we end up with our conclusions and discussion in Section 5.

## 2. BBH MERGER EVENTS

The LVK gravitational wave detector network has completed three rounds of observation operations (O1/O2/O3) as of March 27, 2020 (Abbott et al. 2018, 2021a, 2023a). It began the fourth observing run on May 24, 2023. The online GWTC is a cumulative set of gravitational wave transients maintained by the LVK collaboration. It contains confirmed GW events with a credible probability of being of astrophysical origin ( $p_{astro} > 0.5$ ), which are unlikely due to instrumental noise. Totally 90 confident GW events are included in the catalog as of March 27, 2020. Note that in 7 events, the mass of at least one binary member is not massive enough (Abbott et al. 2018) to be definitely identified as a black hole. In other words, these 7 events might be generated by binary neutron star mergers or neutron star-BH mergers. Since we are only interested in BBH mergers here, we exclude these GW events in our analyses.

Recently, the LVK collaboration specially reported a new GW event, GW230529\_181500, detected during a preliminary analysis of the O4 data (Abac et al. 2024b). It seems to be produced by the coalescing of a less massive compact binary, with the masses of the two objects ranging in  $2.5 - 4.5 M_{\odot}$  and  $1.2 - 2.0 M_{\odot}$ . As a typical lower mass gap system, it is widely believed that the compact stars involved are neutron stars, although the possibility that they are BHs still cannot be excluded (Huang et al. 2024). Considering this uncertainty, we do not include the event in our study.

To sum up, we have 83 GW events in which all the compact objects are confirmed BHs. Our sample is composed of these BHs. Note that 83% of the BBHs in our sample have a false

alarm rate (FAR) less than 1 per year, and 100% of them have a  $p_{astro}$  larger than 0.5.

For each GW event, we denote the mass of the heavier companion as  $m_1$  and the mass of the lighter BH as  $m_2$ . The mass of the final product of the merger, i.e. the newly born massive BH, is denoted as  $m_f$ . Note that during the GW observation of a merger event, the unknown spin of each black hole will affect the estimated BH masses. In the GWTC catalog, the BH masses are estimated based on the assumption that the BH spins are in accordance with the angular speed of the innermost stable circular orbit. For a GW event, the chirp mass and mass ratio  $q$  can be derived from the waveform information. The values of  $m_1$ ,  $m_2$  and  $m_f$  can then be determined from the chirp mass and  $q$  (Poisson & Will 1995; Hannam et al. 2013). To assess the event density of BBH mergers, we need the redshift ( $z$ ) information, which is also available in the GWTC catalog (Abbott et al. 2018). The relevant parameters of these BHs have been taken from the GWTC website and are listed in Table 1 (Abbott et al. 2016a, 2021a, 2023a).

All the confirmed BHs are further divided into two samples. The first sample is called the pre-merger sample ( $S_{pre}$ ), which includes all the separate black holes in the binary systems before the merging process. So, the number of BHs in the  $S_{pre}$  sample is  $83 \times 2 = 166$ . It represents one part of the confirmed BHs once existed in the universe. The second sample is called the post-merger sample ( $S_{post}$ ), which includes all the BHs produced after the merger. The number of BHs in the  $S_{post}$  sample is simply 83. It represents the newly born BHs observed in the universe, which can also be regarded as a sample of stellar BHs at the relatively higher mass segment. Figure 1 plots the distribution of the two samples of BHs on the mass-redshift plane.

In our study, we assume a flat  $\Lambda$ -CDM cosmology with the Hubble parameter and the density

parameters taken as  $H_0 = 67.9 \text{ km s}^{-1} \text{ Mpc}^{-1}$ ,  $\Omega_m = 0.3065$ , and  $\Omega_\Lambda = 0.6935$ . It is consistent with the cosmology parameters taken by the LVK collaboration (Planck Collaboration et al. 2016; Abbott et al. 2018, 2023a).

### 3. THE NON-PARAMETRIC METHOD

The mass function and number density of BHs can be inferred from the observed BH samples given that the BH masses and redshifts are available. However, note that the BH samples are truncated due to the detection threshold of the GW detectors. Similar to previous studies, an event is regarded as being credibly identified when the observed signal to noise ratio (SNR) is no less than 8. In Figure 1, the dashed line shows the truncation line, which represents the maximum redshift of BHs with a certain mass that the upgraded (A+) Advanced LIGO can detect when the SNR is no less than 8 (Chen et al. 2021; Evans et al. 2021). The observational bias caused by this truncation line should be considered when we try to reconstruct the intrinsic distributions of BHs based on the observational data.

The BHs form a bivariate sample with two truncated parameters, i.e. mass ( $m$ ) and redshift ( $z$ ). The joint distribution of BHs is a function of both mass and distance, which can be written as  $\Psi(m, z)$ . If the dependence of the joint distribution on the two parameters is independent of each other, then we have  $\Psi(m, z) = \psi(m)\phi(z)$ , where  $\psi(m)$  represents the mass function and  $\phi(z)$  represents the redshift distribution of black holes. The Lynden-Bell's  $C^-$  method (Lynden-Bell 1971) is suitable for dealing with such mutually independent bivariate problems, which can help obtain the number density of the black holes. Therefore, ensuring the independence of the bivariate truncated data is the basis for us to get a meaningful statistical results from the BBH mass and redshift observations (Efron & Petrosian 1992, 1999).

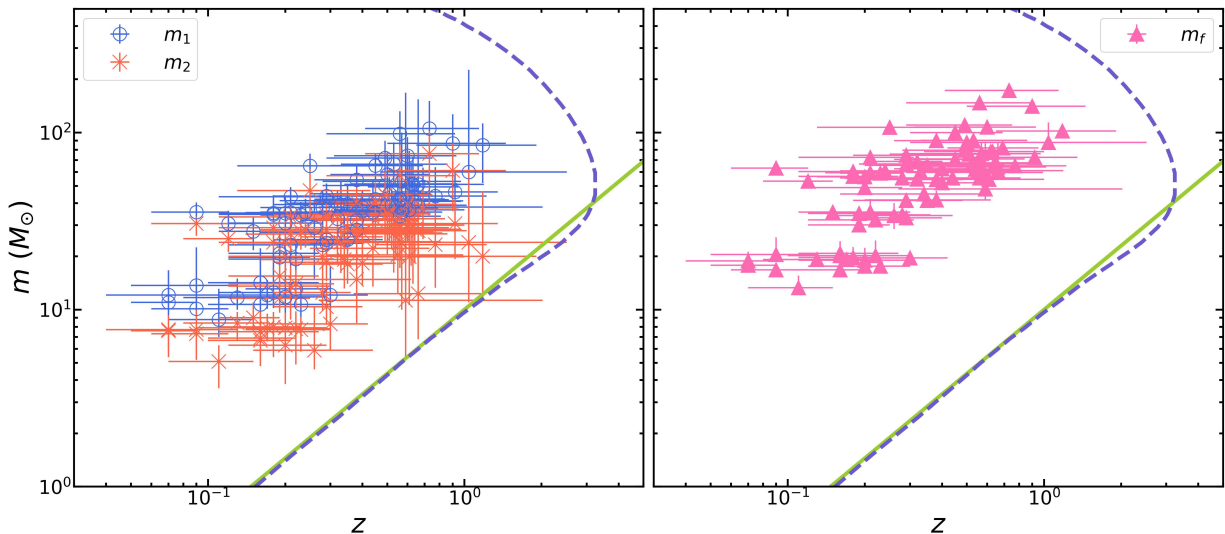


**Figure 1.** Distribution of the black hole masses and redshifts. Left panel: mass versus redshift for the pre-merger sample. The crosses and hollow circles represent the lighter ( $m_2$ ) and heavier ( $m_1$ ) black holes, respectively. Right panel: mass versus redshift for the post-merger sample. In both panels, the dashed line represents the truncation limit and the solid line is the baseline used in our statistical analysis.

In Figure 1, there is a clear positive correlation between the observed mass and redshift for both the pre-merger sample and the post-merger sample. This may be caused by the observational selection effect (Hirai & Mandel 2021; Okano & Suyama 2023; Karathanasis et al. 2023). A GW detector has a limited sensitivity. It can sensitively record nearby GW events. But for distant mergers, it can only detect those events involving relatively massive BHs. Such an observational selection effect also needs to be corrected for before drawing firm conclusions on the intrinsic distribution of BHs.

Therefore, in this section, we first introduce the method to remove the dependence between mass and redshift and then describe how to apply the Lynden-Bell’s  $C^-$  method to bivariate independent parameter samples to obtain the BH mass function, redshift distribution and number density.

### 3.1. The method of $\tau$ statistics

The non-parametric  $\tau$  statistic method (Efron & Petrosian 1992, 1999) can be applied to remove the bias caused by observational selection effects, i.e. the induced correlation between  $m$

and  $z$ . When this method is used in other fields such as gamma-ray bursts and fast radio bursts, it is usually assumed that a power-law relation exists between the luminosity and the redshift due to the observational selection effects (Conselice et al. 2020; Babak et al. 2023). Similarly, in this study, we use  $m \propto (1+z)^\gamma$  to represent the biased dependence of mass on the redshift, where  $\gamma$  is a constant. Once the power-law index  $\gamma$  is determined, we then can correct the mass as  $m' = m/(1+z)^\gamma$ . In this way, we can get the independent parameter pair of  $m'$  and  $z$ , which means the BH distribution function can be expressed as  $\Psi(m', z) = \psi(m')\phi(z)$ .

The value of  $\gamma$  could be determined from the observational data. For a specific  $\gamma$ , the observed data point of each black hole will change from  $(z_i, m_i)$  to the corrected point of  $(z_i, m'_i)$ . For the  $i$ th data point  $(z_i, m'_i)$  in the BH sample, we first define a data set  $J_i$  as

$$J_i = \{j | m'_j \geq m'_i, z_j \leq z_i^{\max}\}, \quad (1)$$

where  $m'_i$  is the corrected mass of the  $i$ th BH and  $z_i^{\max}$  is the maximum redshift at which a BH with mass  $m'_i$  can be detected by the detector. The number of BHs contained in this

region is denoted as  $n_i$ , and the number of BHs with redshift  $z$  less than or equal to  $z_i$  in this region is designated as  $R_i$ . The  $\tau$  test statistic is expressed as

$$\tau \equiv \frac{\sum_i (R_i - E_i)}{\sqrt{\sum_i V_i}}, \quad (2)$$

where  $E_i = \frac{1+n_i}{2}$  and  $V_i = \frac{(n_i-1)^2}{12}$  are the expected mean value and the variance of  $R_i$ , respectively.

According to the  $\tau$  statistic test, if  $R_i$  is uniformly distributed between 1 and  $n_i$ , then the probability of  $R_i \leq E_i$  and  $R_i \geq E_i$  should be nearly equal so that we have  $\tau = 0$ . In this case, we could know that the distribution of mass and redshift are independent of each other. It means that the assumed  $\gamma$  value can correctly remove the bias introduced by the observational selection effect. On the other hand, if  $\tau$  does not equal zero, then we need to adjust the value of  $\gamma$ . The above calculation process is repeated until  $\tau = 0$  is satisfied and the correct  $\gamma$  value is determined.

During the calculations, the truncation line is a key ingredient which is used to calculate  $z_i^{\max}$ . However, note that the truncation line in Figure 1 is a complex function which could not be described by a simple analytical equation. Luckily, for our BH samples, the limit curve in the  $z > 1$  region does not have any impact on the statistics of the non-parametric method. Consequently, we are only concerned about the limit curve in the  $z < 1$  segment. In this region, we notice that the limit curve in fact could be well represented by a simple straight line of  $m = 10z^{1.2}$  (i.e. the solid line in the figure). So, we use this straight line as the effective truncation limit to perform our calculations.

Using this method of  $\tau$  statistics, we finally get the best value as  $\gamma = 2.72_{-0.32}^{+0.31}$  for the pre-merger sample and  $\gamma = 2.63_{-0.38}^{+0.37}$  for the post-merger sample. The observed BH masses are

then corrected by dividing them with  $(1+z)^\gamma$ . The distributions of the BHs after correction are shown in Figure 2. It can be seen that the masses of the black holes no longer show any correlation with the redshifts.

### 3.2. The Lynden-Bell's $C^-$ method

The Lynden-Bell's  $C^-$  method is an effective way to derive the bivariate distributions of astronomical objects from the truncated data. In Equation (1), the number of BHs in the region of  $J_i$  is  $n_i$ . The Lynden-Bell's  $C^-$  method does not include the  $i$ th BH in the analysis, which means the BH number is smaller by 1, i.e.  $N_i = n_i - 1$ . This is the reason that the method is called the " $C^-$ " method (Lynden-Bell 1971). To carry out the calculations, we need to further define another set as

$$J'_i = \{j | m'_j \geq m_i^{\min}, z_j < z_i\}, \quad (3)$$

where  $m_i^{\min}$  is the limit mass at the redshift  $z_i$ . We denote the number of BHs in  $J'_i$  as  $M_i$ .

According to the Lynden-Bell's  $C^-$  method, the cumulative mass function can then be calculated as (Lynden-Bell 1971; Efron & Petrosian 1992)

$$\psi(m'_i) = \prod_{j>i} \left(1 + \frac{1}{N_j}\right), \quad (4)$$

where  $j > i$  means that the operation applies to all BHs whose mass  $m'_j$  is larger than  $m'_i$ . Similarly, the cumulative redshift distribution  $\phi(z)$  can be expressed as

$$\phi(z_i) = \prod_{j<i} \left(1 + \frac{1}{M_j}\right), \quad (5)$$

where  $j < i$  means that the operation applies to all BHs whose redshift  $z_j$  is less than  $z_i$ .

The number density of BHs can be written as

$$\rho_{BH}(z) = \frac{d\phi(z)}{dz} (1+z) \left(\frac{dV(z)}{dz}\right)^{-1}, \quad (6)$$

where the term of  $(1+z)$  results from the cosmological time dilation and  $dV(z)/dz$  is the differential comoving volume which can be further

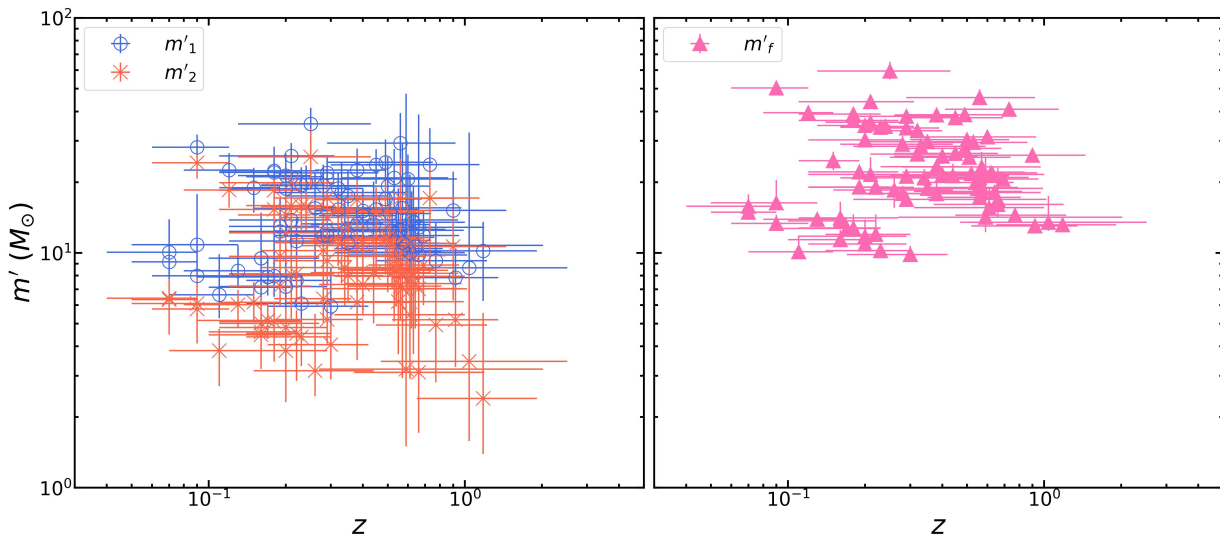


**Figure 2.** Distribution of the black hole masses and redshifts after correcting for the selection effect. Left panel: mass versus redshift for the pre-merger sample. The crosses and hollow circles represent the lighter ( $m_2$ ) and heavier ( $m_1$ ) black holes, respectively. Right panel: mass versus redshift for the post-merger sample.

expressed as (Khokhriakova & Popov 2019)

$$\frac{dV(z)}{dz} = \frac{c}{H_0} \frac{4\pi d_l^2(z)}{(1+z)^2} \frac{1}{\sqrt{\Omega_\Lambda + \Omega_m(1+z)^3}}. \quad (7)$$

Note that the comoving volume at a redshift of  $z$  is  $V = 4\pi D_M^3/3$ , where the comoving distance is  $D_M = d_l/(1+z)$  (Hogg 1999).

### 3.3. Test of the method

The GW observation can be approximately modelled as a threshold process of the observed SNR, which itself depends not only on the GW parameters but also on the specific noise (Fishbach et al. 2018; Mandel et al. 2019; Essick & Fishbach 2024; Gerosa & Bellotti 2024). So the observed distribution cannot be simply modelled as a truncated version of the intrinsic one without introducing a significant bias.

To assess the credibility of our method and the reliability of the results, we have performed simulation tests by using completely simulated samples. For this purpose, we first assume an intrinsic number density of  $\rho(z) \propto z^{-2.0}$ . The number density is then combined with the observed mass function (see results in the next section) to generate a mock BBH sample of 1000

events through Monte Carlo simulations. The distribution of the mock BBHs on the mass-redshift plane is shown in the left panel of Figure 3. The non-parametric method described above is then used to analyze the mock, trying to reconstruct the underlined number density. The reconstructed results are shown in the right panel of Figure 3. In this case, the best-fit power-law function for the number density is  $\rho(z) \propto z^{-1.94 \pm 0.15}$ , which is well consistent with the pre-assumed function of  $\rho(z) \propto z^{-2.0}$ .

In fact, we have also assumed the number density as  $\rho(z) \propto z^{-1.8}$  and  $\rho(z) \propto z^{-2.2}$  in two other simulations. The recovered number density function is  $\rho(z) \propto z^{-1.83 \pm 0.18}$  and  $\rho(z) \propto z^{-2.22 \pm 0.13}$ , respectively. In all these cases, we see that the non-parametric method can satisfactorily re-construct the pre-assumed number density function, which means the method is effective and reliable.

## 4. RESULTS

We have applied the unbiased non-parametric  $\tau$  statistics method on the pre-merger and post-merger BH samples to correct for the dependence between mass and redshift of BHs in-

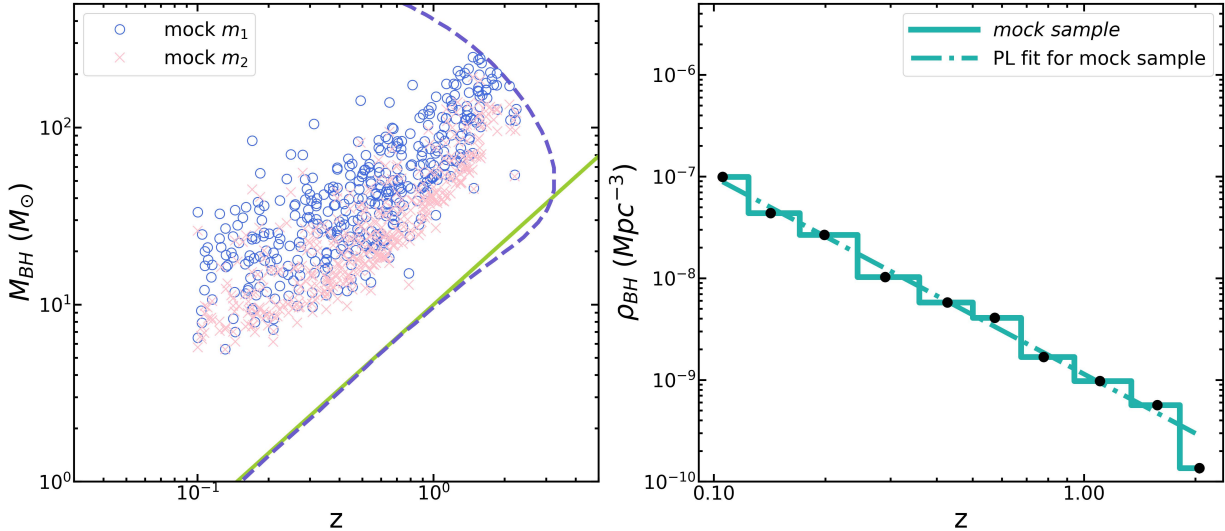


**Figure 3.** Testing the non-parametric method by using completely simulated BBH events. Left panel: distribution of the mock BHs on the mass-redshift plane. The crosses and hollow circles represent the lighter (mock  $m_2$ ) and heavier (mock  $m_1$ ) black holes, respectively. Right panel: number density versus redshift derived from the mock BHs. The dash-dotted line represents the best-fit power-law function.

duced by the observational selection effects. The Lynden-Bell’s  $C^-$  method is then used to derive the intrinsic mass function and redshift distribution of BHs based on the two samples. Additionally, the number density of BHs in the Universe is inferred by considering the redshift information of the BHs. Here we present our numerical results as follows.

#### 4.1. Mass distribution function

The mass distribution function of BHs can be calculated by using Equation (4). The results derived from the pre-merger sample and the post-merger sample are shown in Figure 4. We see that for both samples, the mass function shows a decreasing trend with the increasing mass. However, it is obvious that the mass distribution of the pre-merger sample is different from that of the post-merger sample. In the former case, the mass is mainly distributed between  $2 M_\odot$  and  $40 M_\odot$ ; while it is in a range of  $10 M_\odot - 60 M_\odot$  in the latter case. It clearly shows that the post-merger BHs are significantly more massive.

We have used a simple broken power-law function to fit the mass distribution function, i.e.

$$f(m) \propto \begin{cases} (m/m_b)^\alpha, & m \leq m_b, \\ (m/m_b)^\beta, & m > m_b, \end{cases} \quad (8)$$

where  $m_b$  is the mass at the broken position,  $\alpha$  and  $\beta$  are the two power-law indices characterizing the steepness of the mass function before and after the broken. The best fitting results of the pre-merger sample are  $\alpha = -0.74 \pm 0.21$ ,  $\beta = -4.32 \pm 0.58$ , and  $m'_b = 14.24 \pm 1.06 M_\odot$ . For the post-merger sample, the best fitting results are  $\alpha = -1.2 \pm 0.42$ ,  $\beta = -4.65 \pm 1.15$ , and  $m'_b = 29.31 \pm 3.61 M_\odot$ . The results are shown by the dashed lines in Figure 4. We see that the broken mass of  $m'_b$  of the post-merger sample is significantly larger than that of the pre-merger sample. This is easy to understand since the BHs in the post-merger sample are generally more massive. It is interesting to note that the power-law index in the high mass segment, i.e.  $\beta$ , is generally consistent with each other for the two samples, which means that the mass function of BHs has a steep index of  $\beta \approx -4 - -5$ . On the other hand, the index of  $\alpha$  is clearly dif-



ferent for the two samples. The reason may be that there are too few less massive BHs in the post-merger sample.

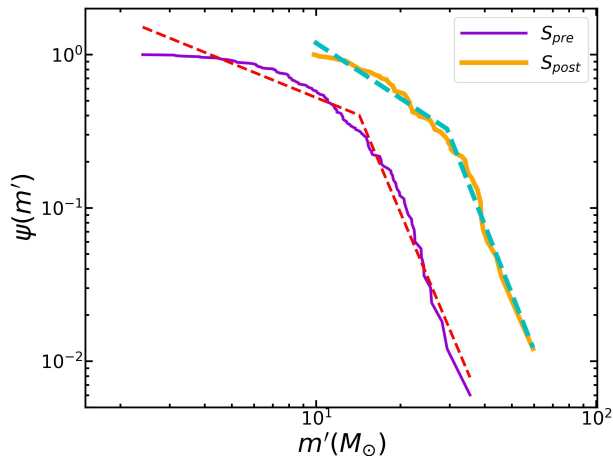


**Figure 4.** Mass function of BHs. The thin solid line represents the pre-merger sample and the thick solid line represents the post-merger sample. Both samples are normalized by the maximum value of the function, respectively. The thin and thick dashed lines represent the best fitting results by using a broken power-law function correspondingly.

Different structures can be identified in the mass distribution of BBHs. For example, it can be modelled with a broken power-law function, a power-law function with a sharp high-mass cut-off, or a Gaussian feature superposed on a power-law function (Abbott et al. 2019, 2021b). Our sample is still relatively small, which only contains 83 BBH merger events. Although our results strongly support the broken power-law model for the mass function, we would like to point out that other models such as a power-law function plus a Gaussian component or a more complex model still cannot be ruled out due to the very limited sample size. A significantly expanded sample available in the future would be helpful in this aspect.

Abbott et al. (2021b) noticed that the distribution of the primary mass of the observed BBH events can be described by a broken power-law function, with a broken mass of  $39.7_{-9.1}^{+20.3} M_{\odot}$ .

It could also be modelled by a Gaussian component peaking at  $33_{-5.6}^{+4.0} M_{\odot}$ , superposed on a power-law function. In our study, as shown in Figure 4, the mass function of the pre-merger BHs is better described by a broken power-law function, with a broken mass of  $m'_b = 14.24 \pm 1.06 M_{\odot}$ . Note that  $m'_b$  here is the de-evolved mass (after correcting for the redshift evolution). The original broken mass is actually  $m_b = m'_b(1+z)^{2.72}$  (see Section 3.1). Taking the average redshift of all the BBHs as  $z = 0.38$ , we get  $m_b = 34.2 \pm 3.8 M_{\odot}$ . This broken mass is interestingly comparable to the characteristic mass reported by Abbott et al. (2021b).

#### 4.2. Redshift distribution and number density of BHs

The cumulative redshift distribution of the two BH samples can be calculated by using Equation (5). The results are shown in Figure 5. We see that the cumulative distribution is almost identical for the two samples. This is easy to understand, since each post-merger BH corresponds to two pre-merger BHs at a particular redshift. Also, it is interesting to note that the cumulative distribution increases rapidly at two redshifts, i.e.  $z \sim 0.2$  and  $z \sim 0.55$ . It indicates that there are more BHs at these two distances.

After obtaining the redshift distribution, we have further calculated the number density of black holes by using Equation (6). The number density is plot versus redshift in Figure 6 for the two BH samples. We see that for both BH samples, the number density decreases steadily as the redshift increases. The behavior can be well fitted by a power-law function in the form of  $\rho(z) \propto z^B$ , where  $B$  is the power-law index. For the pre-merger sample, the best-fit value is  $B \sim -2.12 \pm 0.04$ . For the post-merger sample, we have  $B \sim -2.06 \pm 0.04$ . Interestingly, these two indices are consistent with each other, suggesting that the number density of BHs in the two samples has a similar redshift dependence.

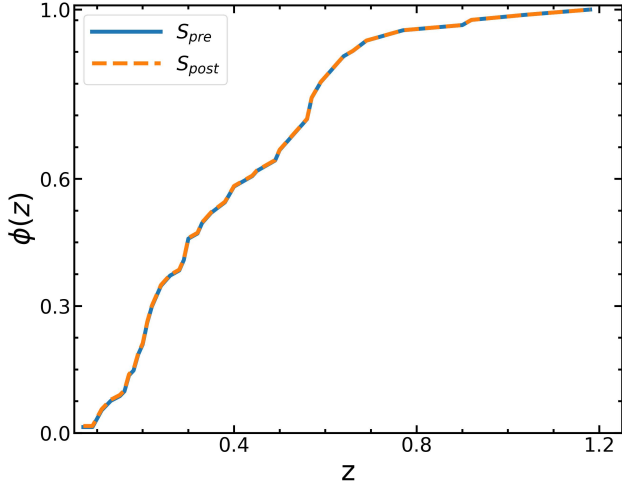


**Figure 5.** Cumulative redshift distribution of BHs. The solid line represents the pre-merger sample and the dashed line represents the post-merger sample. The two curves are essentially overlapped with each other.

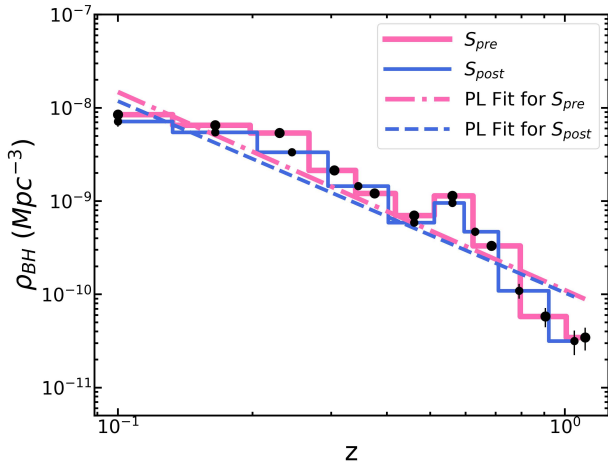


**Figure 6.** The number density of BHs versus redshift. The thick step line represents the pre-merger sample and the thin step line represents the post-merger sample. The dash-dotted line and the dashed line represent the best fitting results of the pre-merger sample and the post-merger sample, respectively, by using a simple power-law function.

Furthermore, from Figure 6, we can notice that the number density has a slight excess at  $z \sim 0.2 - 0.3$  and  $z \sim 0.5 - 0.6$ , which is exactly the reason that leads to the two rapidly increasing episodes illustrated in Figure 5.

#### 4.3. Further test of the method by expanding the sample

Following Fishbach et al. (2020), we have generated a much larger mock BBH sample to further examine the credibility of our method. For each merger event in the observed sample (which includes 83 BBHs), we randomly take 50 SNR values from a normal distribution centered at the true SNR to generate the mock SNRs. The resulting sample contains 4150 mock BBHs. Similar to Fishbach et al. (2020), the masses and redshifts of the mock BBHs are randomly evaluated. The distribution of the mock BBH sample on the mass-redshift plane is shown in the left panel of Figure 7. The non-parametric method is then applied to analyze the mock sample. The number density derived from the mock sample is shown in the right panel of Figure 7. The best-fit power-law index of the plot is  $\sim -2.03 \pm 0.05$ , which is consistent with the result ( $B \sim -2.12 \pm 0.04$ , see Section 4.2) derived from the real observed sample. From this test, it is quite clear that the non-parametric method is very effective and credible in analyzing the BBH GW event data.

As mentioned earlier in Section 3.1, a pre-determined truncation line is necessary in the practice of the non-parametric method. The truncation line is affected by many factors concerning the instrumentation and observation, thus is always ambiguous to some extent. Luckily, it would not affect the final result significantly as long as most of the observational data points are above the adopted truncation line on the  $M_{BH}-z$  plane. In fact, the influence of the truncation line has been examined in many similar applications of the non-parametric method in other field such as gamma-ray bursts (Dainotti et al. 2021; Dong et al. 2022). It is found that the final result is not sensitive to the set up of the truncation line.

## 5. CONCLUSIONS AND DISCUSSION

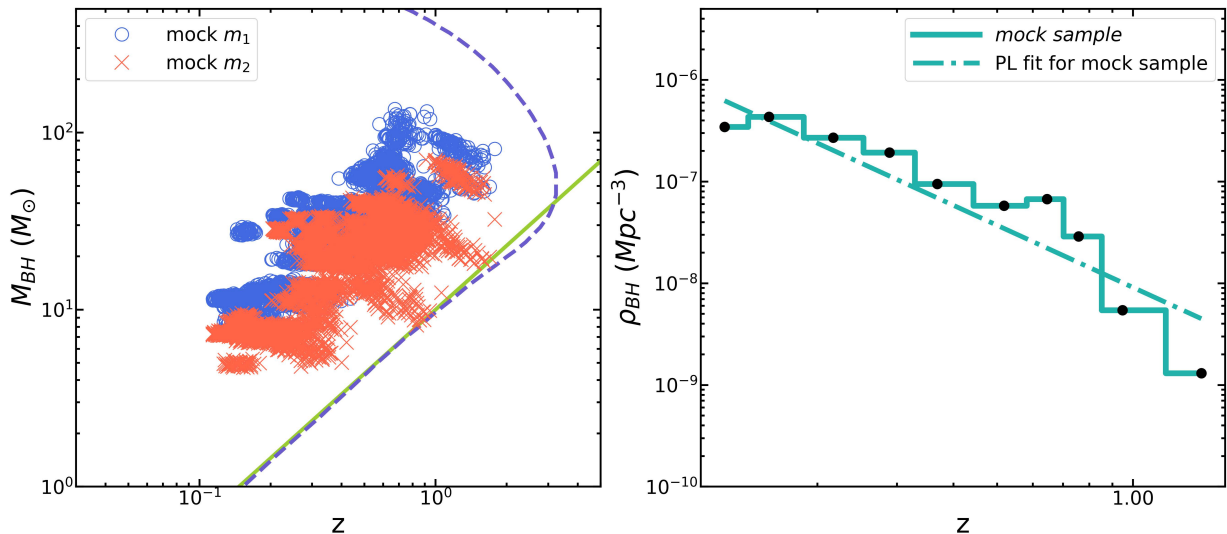


**Figure 7.** Testing the non-parametric method by expanding the observed BBH sample to a much larger mock BBH sample. Left panel: distribution of the mock BHs on the mass-redshift plane. The crosses and hollow circles represent the lighter (mock  $m_2$ ) and heavier (mock  $m_1$ ) black holes, respectively. Right panel: number density versus redshift derived from the mock BHs. The solid step line represents the results derived directly by using our method. The dash-dotted line represents the best-fit power-law function.

Ninety credible GW events are released in the GWTC catalogue by the LVK collaboration, among which 83 cases are confirmed binary black hole mergers. In this study, we have carried out a statistical analysis on the masses and redshifts of these BHs. Two samples consisted of the 166 pre-merger BHs and the 83 post-merger BHs are considered separately, with the former sample representing BHs that once exist in the Universe and the latter representing newly born BHs. The non-parametric  $\tau$  statistic method is adopted to remove the bias caused by observational selection effect. The sensitivity curve of upgraded (A+) Advanced LIGO is used to calculate the truncation line. The derived dependence between redshift and mass are  $m \propto (1+z)^{2.72}$  for the pre-merger sample and  $m \propto (1+z)^{2.63}$  for the post-merger sample. After correcting for the selection effect, the mass and redshift become two independent parameters for the two samples, based on which meaningful statistical analysis can be carried out. Using the Lynden-Bell’s  $C^-$  method, it is found that the mass distribu-

tion can be expressed as a broken power-law function for both samples. In the case of the pre-merger sample, the power-law indices are  $\alpha = -0.74 \pm 0.21$  and  $\beta = -4.32 \pm 0.58$  in the smaller mass region and the higher mass region, respectively, with the break occurring at  $m'_b = 14.24 \pm 1.06 M_\odot$ . For the post-merger sample, the indices are  $\alpha = -1.2 \pm 0.42$  and  $\beta = -4.65 \pm 1.15$  correspondingly, with the broken mass being  $m'_b = 29.31 \pm 3.61 M_\odot$ . We notice that the power-law index  $\beta$  in the higher mass region is essentially identical for the two samples. Additionally, the number density of BHs is derived as  $\rho(z) \propto z^{-2.06} - z^{-2.12}$  from the two samples.

The merger rate of binary black hole systems has been explored by many groups (Spera et al. 2019; Antonini & Gieles 2020; Abbott et al. 2021b; van Son et al. 2022; He et al. 2023; Fishbach & Fragione 2023; Cui & Li 2023; Fakhry 2024), with different conclusions being reached. For example, Conselice et al. (2020) studied the merger process of black holes in ultra low-mass dwarf galaxies. Although their merger rate is

high enough to account for the gravitational wave events detected by LIGO/Virgo, a special feature of their results is that the rate increases with the increasing redshift under various time delay assumptions. On the other hand, Vijaykumar et al. (2024) argued that if BBHs were hosted by a sample of galaxies purely weighted by their stellar mass, then the BBH number density would roughly decrease with the increasing redshift as  $(1+z)^{-0.64}$ . The different outcomes on BBH rates may result from different assumptions and different samples being used. It also reflects the complexity of this difficult problem. In our study, we have used a non-parametric method in which as fewer assumptions are made as possible. Additionally, our study is based on the unified GW events detected by the LVK collaboration. So, it is a beneficial attempt on this issue.

According to our study, the number density of BHs scales with the redshift as  $\rho(z) \propto z^{-2.06} - z^{-2.12}$ , which indicates that the number density decreases with the increasing redshift. It is interesting to note that Abbott et al. (2023b) found that the rate of BBH mergers is proportional to  $(1+z)^{2.9+1.7}_{-1.8}$ , i.e. increasing with redshift. Since the bases of the two power-law expressions are different (i.e.  $z$  versus  $1+z$ ), a direct comparison of the two power-law indices is not available. Here we would like to point out that Abbott et al.'s expression actually corresponds to the term of  $\frac{d\phi(z)}{dz}$  in our Equation 6. It differs with  $\rho(z)$  by a factor of  $(1+z)\left(\frac{dV(z)}{dz}\right)^{-1}$ , which is a complicated term involving the redshift (see Equations (6) and (7)). Additionally, our expression refers to the transformed (and de-correlated) samples, which further explains the huge difference between our index and the index reported by Abbott et al. (2023b).

It deserves mentioning that the BHs in our post-merger samples are universally produced via the merging of two smaller BHs. However, the origin of the BHs in the pre-merger sam-

ple is uncertain. Theoretically, they could come from direct collapse of old massive stars, growth of less massive BHs through accretion, or merging of two BHs. The similarity of some features between the two samples, such as the consistent power-law index  $\beta$  of the mass distribution function in the higher mass region, and the almost equal power-law index  $B$  of the number density, could potentially provide interesting information on the origin of the pre-merger BHs. It points to the possibility that the majority of them, especially those at the higher mass end, should also be of merger origin. However, note that  $S_{pre}$  and  $S_{post}$  are not independent samples because they are filtered in the same way. Especially, the masses of  $S_{post}$  are connected to the masses of  $S_{pre}$ . This may also be part of the reason that the results of post-merger sample and pre-merger sample are similar. Meanwhile, the number of BHs in the two samples is still very limited currently. The fourth observing run (O4) of LVK is still in progress. When it ends in February 2025, the total number of detected GW events is expected to exceed 200. A much larger catalogue of BBHs will be available, which will be helpful for us to further explore the origin and distribution of BHs in the Universe.

## 6. ACKNOWLEDGEMENTS

We thank the anonymous referee for useful comments and suggestions that led to an overall improvement of this study. We are grateful to Yi-Han Iris Yin for helpful discussions. This study was supported by the National Natural Science Foundation of China (Grant Nos. 12233002, U2031118), by the National SKA Program of China No. 2020SKA0120300, by the National Key R&D Program of China (2021YFA0718500). LXJ acknowledges the support by Shandong Provincial Natural Science Foundation (Grant No. ZR2023MA049). YFH also acknowledges the support from the Xinjiang Tianchi Program.

## REFERENCES

- Abac, A. G., Abbott, R., Abe, H., et al. 2024a, *ApJ*, 973, 132, doi: [10.3847/1538-4357/ad65ce](https://doi.org/10.3847/1538-4357/ad65ce)
- Abac, A. G., Abbott, R., Abouelfettouh, I., et al. 2024b, *ApJL*, 970, L34, doi: [10.3847/2041-8213/ad5beb](https://doi.org/10.3847/2041-8213/ad5beb)
- Abbott, B. P., Abbott, R., Abbott, T. D., et al. 2016a, *PhRvL*, 116, 061102, doi: [10.1103/PhysRevLett.116.061102](https://doi.org/10.1103/PhysRevLett.116.061102)
- . 2016b, *Physical Review X*, 6, 041015, doi: [10.1103/PhysRevX.6.041015](https://doi.org/10.1103/PhysRevX.6.041015)
- . 2018, *Living Reviews in Relativity*, 21, 3, doi: [10.1007/s41114-018-0012-9](https://doi.org/10.1007/s41114-018-0012-9)
- . 2019, *ApJL*, 882, L24, doi: [10.3847/2041-8213/ab3800](https://doi.org/10.3847/2041-8213/ab3800)
- Abbott, R., Abbott, T. D., Abraham, S., et al. 2021a, *Physical Review X*, 11, 021053, doi: [10.1103/PhysRevX.11.021053](https://doi.org/10.1103/PhysRevX.11.021053)
- . 2021b, *ApJL*, 913, L7, doi: [10.3847/2041-8213/abe949](https://doi.org/10.3847/2041-8213/abe949)
- Abbott, R., Abbott, T. D., Acernese, F., et al. 2023a, *Physical Review X*, 13, 041039, doi: [10.1103/PhysRevX.13.041039](https://doi.org/10.1103/PhysRevX.13.041039)
- . 2023b, *Physical Review X*, 13, 011048, doi: [10.1103/PhysRevX.13.011048](https://doi.org/10.1103/PhysRevX.13.011048)
- Acernese, F., Agathos, M., Agatsuma, K., et al. 2015, *Classical and Quantum Gravity*, 32, 024001, doi: [10.1088/0264-9381/32/2/024001](https://doi.org/10.1088/0264-9381/32/2/024001)
- Akutsu, T., Ando, M., Araki, S., et al. 2018, *Progress of Theoretical and Experimental Physics*, 2018, 013F01, doi: [10.1093/ptep/ptx180](https://doi.org/10.1093/ptep/ptx180)
- Ali-Haïmoud, Y., Kovetz, E. D., & Kamionkowski, M. 2017, *PhRvD*, 96, 123523, doi: [10.1103/PhysRevD.96.123523](https://doi.org/10.1103/PhysRevD.96.123523)
- Antonini, F., & Gieles, M. 2020, *PhRvD*, 102, 123016, doi: [10.1103/PhysRevD.102.123016](https://doi.org/10.1103/PhysRevD.102.123016)
- Antonini, F., Toonen, S., & Hamers, A. S. 2017, *ApJ*, 841, 77, doi: [10.3847/1538-4357/aa6f5e](https://doi.org/10.3847/1538-4357/aa6f5e)
- Babak, S., Caprini, C., Figueroa, D. G., et al. 2023, *JCAP*, 2023, 034, doi: [10.1088/1475-7516/2023/08/034](https://doi.org/10.1088/1475-7516/2023/08/034)
- Banerjee, S., Baumgardt, H., & Kroupa, P. 2010, *MNRAS*, 402, 371, doi: [10.1111/j.1365-2966.2009.15880.x](https://doi.org/10.1111/j.1365-2966.2009.15880.x)
- Bartos, I., Kocsis, B., Haiman, Z., & Márka, S. 2017, *ApJ*, 835, 165, doi: [10.3847/1538-4357/835/2/165](https://doi.org/10.3847/1538-4357/835/2/165)
- Bethe, H. A., & Brown, G. E. 1998, *ApJ*, 506, 780, doi: [10.1086/306265](https://doi.org/10.1086/306265)
- Bird, S., Cholis, I., Muñoz, J. B., et al. 2016, *PhRvL*, 116, 201301, doi: [10.1103/PhysRevLett.116.201301](https://doi.org/10.1103/PhysRevLett.116.201301)
- Callister, T. A., & Farr, W. M. 2024, *Physical Review X*, 14, 021005, doi: [10.1103/PhysRevX.14.021005](https://doi.org/10.1103/PhysRevX.14.021005)
- Carr, B. J., & Hawking, S. W. 1974, *MNRAS*, 168, 399, doi: [10.1093/mnras/168.2.399](https://doi.org/10.1093/mnras/168.2.399)
- Chattopadhyay, D., Hurley, J., Stevenson, S., & Raidani, A. 2022, *MNRAS*, 513, 4527, doi: [10.1093/mnras/stac1163](https://doi.org/10.1093/mnras/stac1163)
- Chattopadhyay, D., Stegmann, J., Antonini, F., Barber, J., & Romero-Shaw, I. M. 2023, *MNRAS*, 526, 4908, doi: [10.1093/mnras/stad3048](https://doi.org/10.1093/mnras/stad3048)
- Chen, H.-Y., Holz, D. E., Miller, J., et al. 2021, *Classical and Quantum Gravity*, 38, 055010, doi: [10.1088/1361-6382/abd594](https://doi.org/10.1088/1361-6382/abd594)
- Chen, Z.-C., Du, S.-S., Huang, Q.-G., & You, Z.-Q. 2023, *JCAP*, 2023, 024, doi: [10.1088/1475-7516/2023/03/024](https://doi.org/10.1088/1475-7516/2023/03/024)
- Conselice, C. J., Bhatawdekar, R., Palmese, A., & Hartley, W. G. 2020, *ApJ*, 890, 8, doi: [10.3847/1538-4357/ab5dad](https://doi.org/10.3847/1538-4357/ab5dad)
- Cui, Z., & Li, X.-D. 2023, *MNRAS*, 523, 5565, doi: [10.1093/mnras/stad1800](https://doi.org/10.1093/mnras/stad1800)
- Dainotti, M., Petrosian, V., Willingale, R., et al. 2015, *MNRAS*, 451, 3898, doi: [10.1093/mnras/stv1229](https://doi.org/10.1093/mnras/stv1229)
- Dainotti, M. G., Petrosian, V., & Bowden, L. 2021, *ApJL*, 914, L40, doi: [10.3847/2041-8213/abf5e4](https://doi.org/10.3847/2041-8213/abf5e4)
- Deng, C.-M., Wei, J.-J., & Wu, X.-F. 2019, *Journal of High Energy Astrophysics*, 23, 1, doi: [10.1016/j.jheap.2019.05.001](https://doi.org/10.1016/j.jheap.2019.05.001)
- Dong, X. F., Li, X. J., Zhang, Z. B., & Zhang, X. L. 2022, *MNRAS*, 513, 1078, doi: [10.1093/mnras/stac949](https://doi.org/10.1093/mnras/stac949)
- Dong, X. F., Zhang, Z. B., Li, Q. M., Huang, Y. F., & Bian, K. 2023, *ApJ*, 958, 37, doi: [10.3847/1538-4357/acf852](https://doi.org/10.3847/1538-4357/acf852)
- Edelman, B., Doctor, Z., Godfrey, J., & Farr, B. 2022, *ApJ*, 924, 101, doi: [10.3847/1538-4357/ac3667](https://doi.org/10.3847/1538-4357/ac3667)
- Edelman, B., Farr, B., & Doctor, Z. 2023, *ApJ*, 946, 16, doi: [10.3847/1538-4357/acb5ed](https://doi.org/10.3847/1538-4357/acb5ed)

- Efron, B., & Petrosian, V. 1992, *ApJ*, 399, 345, doi: [10.1086/171931](https://doi.org/10.1086/171931)
- . 1999, *Journal of the American Statistical Association*, 94, 824
- Essick, R., & Fishbach, M. 2024, *ApJ*, 962, 169, doi: [10.3847/1538-4357/ad1604](https://doi.org/10.3847/1538-4357/ad1604)
- Evans, M., Adhikari, R. X., Afle, C., et al. 2021, arXiv e-prints, arXiv:2109.09882, doi: [10.48550/arXiv.2109.09882](https://doi.org/10.48550/arXiv.2109.09882)
- Fakhry, S. 2024, *ApJ*, 961, 8, doi: [10.3847/1538-4357/ad0e66](https://doi.org/10.3847/1538-4357/ad0e66)
- Farah, A. M., Edelman, B., Zevin, M., et al. 2023, *ApJ*, 955, 107, doi: [10.3847/1538-4357/aced02](https://doi.org/10.3847/1538-4357/aced02)
- Farr, W. M. 2019, *Research Notes of the American Astronomical Society*, 3, 66, doi: [10.3847/2515-5172/ab1d5f](https://doi.org/10.3847/2515-5172/ab1d5f)
- Farr, W. M., Stevenson, S., Miller, M. C., et al. 2017, *Nature*, 548, 426, doi: [10.1038/nature23453](https://doi.org/10.1038/nature23453)
- Fishbach, M., Farr, W. M., & Holz, D. E. 2020, *ApJL*, 891, L31, doi: [10.3847/2041-8213/ab77c9](https://doi.org/10.3847/2041-8213/ab77c9)
- Fishbach, M., & Fragione, G. 2023, *MNRAS*, 522, 5546, doi: [10.1093/mnras/stad1364](https://doi.org/10.1093/mnras/stad1364)
- Fishbach, M., Holz, D. E., & Farr, W. M. 2018, *ApJL*, 863, L41, doi: [10.3847/2041-8213/aad800](https://doi.org/10.3847/2041-8213/aad800)
- Foreman-Mackey, D., Hogg, D. W., & Morton, T. D. 2014, *ApJ*, 795, 64, doi: [10.1088/0004-637X/795/1/64](https://doi.org/10.1088/0004-637X/795/1/64)
- Fragione, G., Leigh, N. W. C., & Perna, R. 2019, *MNRAS*, 488, 2825, doi: [10.1093/mnras/stz1803](https://doi.org/10.1093/mnras/stz1803)
- Gallegos-Garcia, M., Berry, C. P. L., Marchant, P., & Kalogera, V. 2021, *ApJ*, 922, 110, doi: [10.3847/1538-4357/ac2610](https://doi.org/10.3847/1538-4357/ac2610)
- Gerosa, D., & Bellotti, M. 2024, *Classical and Quantum Gravity*, 41, 125002, doi: [10.1088/1361-6382/ad4509](https://doi.org/10.1088/1361-6382/ad4509)
- Giacobbo, N., & Mapelli, M. 2018, *MNRAS*, 480, 2011, doi: [10.1093/mnras/sty1999](https://doi.org/10.1093/mnras/sty1999)
- Gong, C., Zhu, T., Niu, R., et al. 2022, *PhRvD*, 105, 044034, doi: [10.1103/PhysRevD.105.044034](https://doi.org/10.1103/PhysRevD.105.044034)
- Hannam, M., Brown, D. A., Fairhurst, S., Fryer, C. L., & Harry, I. W. 2013, *ApJL*, 766, L14, doi: [10.1088/2041-8205/766/1/L14](https://doi.org/10.1088/2041-8205/766/1/L14)
- He, J.-G., Shao, Y., Gao, S.-J., & Li, X.-D. 2023, *ApJ*, 953, 153, doi: [10.3847/1538-4357/ace348](https://doi.org/10.3847/1538-4357/ace348)
- Heinzel, J., Mould, M., Álvarez-López, S., & Vitale, S. 2024, arXiv e-prints, arXiv:2406.16813, doi: [10.48550/arXiv.2406.16813](https://doi.org/10.48550/arXiv.2406.16813)
- Hirai, R., & Mandel, I. 2021, *PASA*, 38, e056, doi: [10.1017/pasa.2021.53](https://doi.org/10.1017/pasa.2021.53)
- Hogg, D. W. 1999, arXiv e-prints, astro-ph/9905116, doi: [10.48550/arXiv.astro-ph/9905116](https://doi.org/10.48550/arXiv.astro-ph/9905116)
- Huang, Q.-G., Yuan, C., Chen, Z.-C., & Liu, L. 2024, *JCAP*, 2024, 030, doi: [10.1088/1475-7516/2024/08/030](https://doi.org/10.1088/1475-7516/2024/08/030)
- Karathanasis, C., Mukherjee, S., & Mastrogiovanni, S. 2023, *MNRAS*, 523, 4539, doi: [10.1093/mnras/stad1373](https://doi.org/10.1093/mnras/stad1373)
- Khokhriakova, A. D., & Popov, S. B. 2019, *Journal of High Energy Astrophysics*, 24, 1, doi: [10.1016/j.jheap.2019.09.004](https://doi.org/10.1016/j.jheap.2019.09.004)
- Kirshner, R. P., Oemler, A., J., & Schechter, P. L. 1978, *AJ*, 83, 1549, doi: [10.1086/112363](https://doi.org/10.1086/112363)
- Kulkarni, S. R., Hut, P., & McMillan, S. 1993, *Nature*, 364, 421, doi: [10.1038/364421a0](https://doi.org/10.1038/364421a0)
- Levine, D., Dainotti, M., Zvonarek, K. J., et al. 2022, *ApJ*, 925, 15, doi: [10.3847/1538-4357/ac4221](https://doi.org/10.3847/1538-4357/ac4221)
- Li, Q. M., Sun, Q. B., Zhang, Z. B., Zhang, K. J., & Long, G. 2024a, *MNRAS*, 527, 7111, doi: [10.1093/mnras/stad3619](https://doi.org/10.1093/mnras/stad3619)
- Li, Y.-J., Wang, Y.-Z., Tang, S.-P., & Fan, Y.-Z. 2024b, *PhRvL*, 133, 051401, doi: [10.1103/PhysRevLett.133.051401](https://doi.org/10.1103/PhysRevLett.133.051401)
- LIGO Scientific Collaboration, Aasi, J., Abbott, B. P., et al. 2015, *Classical and Quantum Gravity*, 32, 074001, doi: [10.1088/0264-9381/32/7/074001](https://doi.org/10.1088/0264-9381/32/7/074001)
- Liu, Z.-Y., Zhang, F.-W., & Zhu, S.-Y. 2021, *Research in Astronomy and Astrophysics*, 21, 254, doi: [10.1088/1674-4527/21/10/254](https://doi.org/10.1088/1674-4527/21/10/254)
- Lloyd-Ronning, N. M., Fryer, C. L., & Ramirez-Ruiz, E. 2002, *ApJ*, 574, 554, doi: [10.1086/341059](https://doi.org/10.1086/341059)
- Loh, E. D., & Spillar, E. J. 1986, *ApJL*, 307, L1, doi: [10.1086/184717](https://doi.org/10.1086/184717)
- Lynden-Bell, D. 1971, *MNRAS*, 155, 95, doi: [10.1093/mnras/155.1.95](https://doi.org/10.1093/mnras/155.1.95)
- Mandel, I., Farr, W. M., Colonna, A., et al. 2017, *MNRAS*, 465, 3254, doi: [10.1093/mnras/stw2883](https://doi.org/10.1093/mnras/stw2883)
- Mandel, I., Farr, W. M., & Gair, J. R. 2019, *MNRAS*, 486, 1086, doi: [10.1093/mnras/stz896](https://doi.org/10.1093/mnras/stz896)
- Martinez, M. A. S., Fragione, G., Kremer, K., et al. 2020, *ApJ*, 903, 67, doi: [10.3847/1538-4357/abba25](https://doi.org/10.3847/1538-4357/abba25)

- McKernan, B., Ford, K. E. S., Lyra, W., & Perets, H. B. 2012, *MNRAS*, 425, 460, doi: [10.1111/j.1365-2966.2012.21486.x](https://doi.org/10.1111/j.1365-2966.2012.21486.x)
- Ng, K. K. Y., Chen, S., Goncharov, B., et al. 2022, *ApJL*, 931, L12, doi: [10.3847/2041-8213/ac6bea](https://doi.org/10.3847/2041-8213/ac6bea)
- Okano, S., & Suyama, T. 2023, *Astrophys. Space Sci.*, 368, 5, doi: [10.1007/s10509-022-04160-4](https://doi.org/10.1007/s10509-022-04160-4)
- Palmese, A., Fishbach, M., Burke, C. J., Annis, J., & Liu, X. 2021, *ApJL*, 914, L34, doi: [10.3847/2041-8213/ac0883](https://doi.org/10.3847/2041-8213/ac0883)
- Pescalli, A., Ghirlanda, G., Salvaterra, R., et al. 2016, *A&A*, 587, A40, doi: [10.1051/0004-6361/201526760](https://doi.org/10.1051/0004-6361/201526760)
- Peterson, B. A., Ellis, R. S., Efstathiou, G., et al. 1986, *MNRAS*, 221, 233, doi: [10.1093/mnras/221.2.233](https://doi.org/10.1093/mnras/221.2.233)
- Planck Collaboration, Ade, P. A. R., Aghanim, N., et al. 2016, *A&A*, 594, A13, doi: [10.1051/0004-6361/201525830](https://doi.org/10.1051/0004-6361/201525830)
- Poisson, E., & Will, C. M. 1995, *PhRvD*, 52, 848, doi: [10.1103/PhysRevD.52.848](https://doi.org/10.1103/PhysRevD.52.848)
- Portegies Zwart, S. F., & McMillan, S. L. W. 2000, *ApJL*, 528, L17, doi: [10.1086/312422](https://doi.org/10.1086/312422)
- Rauf, L., Howlett, C., Stevenson, S., & Riley, J. 2024, arXiv e-prints, arXiv:2406.11885, doi: [10.48550/arXiv.2406.11885](https://doi.org/10.48550/arXiv.2406.11885)
- Rodriguez, C. L., Chatterjee, S., & Rasio, F. A. 2016, *PhRvD*, 93, 084029, doi: [10.1103/PhysRevD.93.084029](https://doi.org/10.1103/PhysRevD.93.084029)
- Sadiq, J., Dent, T., & Wysocki, D. 2022, *PhRvD*, 105, 123014, doi: [10.1103/PhysRevD.105.123014](https://doi.org/10.1103/PhysRevD.105.123014)
- Saini, P., Bhat, S. A., Favata, M., & Arun, K. G. 2024, *PhRvD*, 109, 084056, doi: [10.1103/PhysRevD.109.084056](https://doi.org/10.1103/PhysRevD.109.084056)
- Singal, J., Petrosian, V., Lawrence, A., & Stawarz, L. 2011, *ApJ*, 743, 104, doi: [10.1088/0004-637X/743/2/104](https://doi.org/10.1088/0004-637X/743/2/104)
- Spera, M., Mapelli, M., Giacobbo, N., et al. 2019, *MNRAS*, 485, 889, doi: [10.1093/mnras/stz359](https://doi.org/10.1093/mnras/stz359)
- Tagawa, H., Haiman, Z., Bartos, I., & Kocsis, B. 2020, *ApJ*, 899, 26, doi: [10.3847/1538-4357/aba2cc](https://doi.org/10.3847/1538-4357/aba2cc)
- van Son, L. A. C., de Mink, S. E., Callister, T., et al. 2022, *ApJ*, 931, 17, doi: [10.3847/1538-4357/ac64a3](https://doi.org/10.3847/1538-4357/ac64a3)
- Vigna-Gómez, A., Toonen, S., Ramirez-Ruiz, E., et al. 2021, *ApJL*, 907, L19, doi: [10.3847/2041-8213/abd5b7](https://doi.org/10.3847/2041-8213/abd5b7)
- Vijaykumar, A., Fishbach, M., Adhikari, S., & Holz, D. E. 2024, *ApJ*, 972, 157, doi: [10.3847/1538-4357/ad6140](https://doi.org/10.3847/1538-4357/ad6140)
- Wu, Y. 2020, *PhRvD*, 101, 083008, doi: [10.1103/PhysRevD.101.083008](https://doi.org/10.1103/PhysRevD.101.083008)
- Yu, H., Wang, F. Y., Dai, Z. G., & Cheng, K. S. 2015, *ApJS*, 218, 13, doi: [10.1088/0067-0049/218/1/13](https://doi.org/10.1088/0067-0049/218/1/13)
- Zeng, H., Petrosian, V., & Yi, T. 2021, *ApJ*, 913, 120, doi: [10.3847/1538-4357/abf65e](https://doi.org/10.3847/1538-4357/abf65e)
- Zhang, G. Q., & Wang, F. Y. 2018, *ApJ*, 852, 1, doi: [10.3847/1538-4357/aa9ce5](https://doi.org/10.3847/1538-4357/aa9ce5)

**Table 1.** Key parameters of the black holes in the BBH GW events.

| Name            | $m_1 (M_\odot)$                         | $m_2 (M_\odot)$                        | $m_f (M_\odot)$                         | redshift                               | FAR(year <sup>-1</sup> ) | $p_{astro}$ |
|-----------------|---|--|---|--|--------------------------|-------------|
| GW150914        | 35.6 <sup>+4.7</sup> <sub>-3.1</sub>    | 30.6 <sup>+3.0</sup> <sub>-4.4</sub>   | 63.1 <sup>+3.4</sup> <sub>-3.0</sub>    | 0.09 <sup>+0.03</sup> <sub>-0.03</sub> | 1.00E - 07               | 1.00        |
| GW151012        | 23.2 <sup>+14.9</sup> <sub>-5.5</sub>   | 13.6 <sup>+4.1</sup> <sub>-4.8</sub>   | 35.6 <sup>+10.8</sup> <sub>-3.8</sub>   | 0.21 <sup>+0.09</sup> <sub>-0.09</sub> | 7.92E - 03               | 1.00        |
| GW151226        | 13.7 <sup>+8.8</sup> <sub>-3.2</sub>    | 7.7 <sup>+2.2</sup> <sub>-2.5</sub>    | 20.5 <sup>+6.4</sup> <sub>-1.5</sub>    | 0.09 <sup>+0.04</sup> <sub>-0.04</sub> | 1.00E - 07               | 1.00        |
| GW170104        | 30.8 <sup>+7.3</sup> <sub>-5.6</sub>    | 20.0 <sup>+4.9</sup> <sub>-4.6</sub>   | 48.9 <sup>+5.1</sup> <sub>-4.0</sub>    | 0.20 <sup>+0.08</sup> <sub>-0.08</sub> | 1.00E - 07               | 1.00        |
| GW170608        | 11.0 <sup>+5.5</sup> <sub>-1.7</sub>    | 7.6 <sup>+1.4</sup> <sub>-2.2</sub>    | 17.8 <sup>+3.4</sup> <sub>-0.7</sub>    | 0.07 <sup>+0.02</sup> <sub>-0.02</sub> | 1.00E - 07               | 1.00        |
| GW170729        | 50.2 <sup>+16.2</sup> <sub>-10.2</sub>  | 34.0 <sup>+9.1</sup> <sub>-10.1</sub>  | 79.5 <sup>+14.7</sup> <sub>-10.2</sub>  | 0.49 <sup>+0.19</sup> <sub>-0.21</sub> | 2.00E - 02               | 0.98        |
| GW170809        | 35.0 <sup>+8.3</sup> <sub>-5.9</sub>    | 23.8 <sup>+5.1</sup> <sub>-5.2</sub>   | 56.3 <sup>+5.2</sup> <sub>-3.8</sub>    | 0.20 <sup>+0.05</sup> <sub>-0.07</sub> | 1.00E - 07               | 1.00        |
| GW170814        | 30.6 <sup>+5.6</sup> <sub>-3.0</sub>    | 25.2 <sup>+2.8</sup> <sub>-4.0</sub>   | 53.2 <sup>+3.2</sup> <sub>-2.4</sub>    | 0.12 <sup>+0.03</sup> <sub>-0.04</sub> | 1.00E - 07               | 1.00        |
| GW170818        | 35.4 <sup>+7.5</sup> <sub>-4.7</sub>    | 26.7 <sup>+4.3</sup> <sub>-5.2</sub>   | 59.4 <sup>+4.9</sup> <sub>-3.8</sub>    | 0.21 <sup>+0.07</sup> <sub>-0.07</sub> | 4.20E - 05               | 1.00        |
| GW170823        | 39.5 <sup>+11.2</sup> <sub>-6.7</sub>   | 29.0 <sup>+6.7</sup> <sub>-7.8</sub>   | 65.4 <sup>+10.1</sup> <sub>-7.4</sub>   | 0.35 <sup>+0.15</sup> <sub>-0.15</sub> | 1.00E - 07               | 1.00        |
| GW190403.051519 | 85.0 <sup>+27.8</sup> <sub>-33.0</sub>  | 20.0 <sup>+26.3</sup> <sub>-8.4</sub>  | 102.2 <sup>+26.3</sup> <sub>-24.3</sub> | 1.18 <sup>+0.73</sup> <sub>-0.53</sub> | 7.70E + 00               | 0.61        |
| GW190408.181802 | 24.8 <sup>+5.4</sup> <sub>-3.5</sub>    | 18.5 <sup>+3.3</sup> <sub>-4.0</sub>   | 41.4 <sup>+3.9</sup> <sub>-2.9</sub>    | 0.29 <sup>+0.07</sup> <sub>-0.11</sub> | 1.00E - 05               | 1.00        |
| GW190412        | 27.7 <sup>+6.0</sup> <sub>-6.0</sub>    | 9.0 <sup>+2.0</sup> <sub>-1.4</sub>    | 35.6 <sup>+4.8</sup> <sub>-4.5</sub>    | 0.15 <sup>+0.04</sup> <sub>-0.04</sub> | 1.00E - 05               | 1.00        |
| GW190413.052954 | 33.7 <sup>+10.4</sup> <sub>-6.4</sub>   | 24.2 <sup>+6.5</sup> <sub>-7.0</sub>   | 55.5 <sup>+10.1</sup> <sub>-7.3</sub>   | 0.56 <sup>+0.25</sup> <sub>-0.21</sub> | 8.20E - 01               | 0.93        |
| GW190413.134308 | 51.3 <sup>+16.6</sup> <sub>-12.6</sub>  | 30.4 <sup>+11.7</sup> <sub>-12.7</sub> | 78.0 <sup>+16.1</sup> <sub>-11.5</sub>  | 0.62 <sup>+0.32</sup> <sub>-0.26</sub> | 1.80E - 01               | 0.99        |
| GW190421.213856 | 42.0 <sup>+10.1</sup> <sub>-7.4</sub>   | 32.0 <sup>+8.3</sup> <sub>-9.8</sub>   | 70.5 <sup>+12.4</sup> <sub>-9.0</sub>   | 0.45 <sup>+0.21</sup> <sub>-0.19</sub> | 2.80E - 03               | 1.00        |
| GW190426.190642 | 105.5 <sup>+45.3</sup> <sub>-24.1</sub> | 76.0 <sup>+26.2</sup> <sub>-36.5</sub> | 172.9 <sup>+37.7</sup> <sub>-33.6</sub> | 0.73 <sup>+0.41</sup> <sub>-0.32</sub> | 4.10E + 00               | 0.75        |
| GW190503.185404 | 41.3 <sup>+10.3</sup> <sub>-7.7</sub>   | 28.3 <sup>+7.5</sup> <sub>-9.2</sub>   | 66.5 <sup>+9.4</sup> <sub>-7.9</sub>    | 0.29 <sup>+0.10</sup> <sub>-0.10</sub> | 1.00E - 05               | 1.00        |
| GW190512.180714 | 23.2 <sup>+5.6</sup> <sub>-5.6</sub>    | 12.5 <sup>+3.5</sup> <sub>-2.6</sub>   | 34.3 <sup>+4.1</sup> <sub>-3.4</sub>    | 0.28 <sup>+0.08</sup> <sub>-0.10</sub> | 7.92E - 03               | 1.00        |
| GW190513.205428 | 36.0 <sup>+10.6</sup> <sub>-9.7</sub>   | 18.3 <sup>+7.4</sup> <sub>-4.7</sub>   | 52.1 <sup>+8.8</sup> <sub>-6.6</sub>    | 0.40 <sup>+0.14</sup> <sub>-0.13</sub> | 1.30E - 05               | 1.00        |
| GW190514.065416 | 40.9 <sup>+17.3</sup> <sub>-9.3</sub>   | 28.4 <sup>+10.0</sup> <sub>-10.1</sub> | 66.4 <sup>+19.0</sup> <sub>-11.5</sub>  | 0.64 <sup>+0.33</sup> <sub>-0.30</sub> | 2.80E + 00               | 0.76        |
| GW190517.055101 | 39.2 <sup>+13.9</sup> <sub>-9.2</sub>   | 24.0 <sup>+7.4</sup> <sub>-7.9</sub>   | 60.1 <sup>+9.9</sup> <sub>-9.4</sub>    | 0.33 <sup>+0.26</sup> <sub>-0.15</sub> | 3.50E - 04               | 1.00        |
| GW190519.153544 | 65.1 <sup>+10.8</sup> <sub>-11.0</sub>  | 40.8 <sup>+11.5</sup> <sub>-12.7</sub> | 100.0 <sup>+13.0</sup> <sub>-12.9</sub> | 0.45 <sup>+0.24</sup> <sub>-0.15</sub> | 1.00E - 05               | 1.00        |
| GW190521        | 98.4 <sup>+33.6</sup> <sub>-21.7</sub>  | 57.2 <sup>+27.1</sup> <sub>-30.1</sub> | 147.4 <sup>+40.0</sup> <sub>-16.0</sub> | 0.56 <sup>+0.36</sup> <sub>-0.27</sub> | 1.30E - 03               | 1.00        |
| GW190521.074359 | 43.4 <sup>+5.8</sup> <sub>-5.5</sub>    | 33.4 <sup>+5.2</sup> <sub>-6.8</sub>   | 72.6 <sup>+6.5</sup> <sub>-5.4</sub>    | 0.21 <sup>+0.10</sup> <sub>-0.10</sub> | 1.00E - 05               | 1.00        |
| GW190527.092055 | 35.6 <sup>+18.7</sup> <sub>-8.0</sub>   | 22.2 <sup>+9.0</sup> <sub>-8.7</sub>   | 55.5 <sup>+17.9</sup> <sub>-8.5</sub>   | 0.44 <sup>+0.29</sup> <sub>-0.19</sub> | 1.00E - 07               | 1.00        |
| GW190602.175927 | 71.8 <sup>+18.1</sup> <sub>-14.6</sub>  | 44.8 <sup>+15.5</sup> <sub>-19.6</sub> | 110.5 <sup>+17.9</sup> <sub>-13.9</sub> | 0.49 <sup>+0.26</sup> <sub>-0.20</sub> | 1.00E - 05               | 1.00        |
| GW190620.030421 | 58.0 <sup>+19.2</sup> <sub>-13.3</sub>  | 35.0 <sup>+13.1</sup> <sub>-14.5</sub> | 88.0 <sup>+17.2</sup> <sub>-12.4</sub>  | 0.50 <sup>+0.23</sup> <sub>-0.20</sub> | 1.10E - 02               | 0.99        |
| GW190630.185205 | 35.1 <sup>+6.5</sup> <sub>-5.5</sub>    | 24.0 <sup>+5.5</sup> <sub>-5.2</sub>   | 56.6 <sup>+4.4</sup> <sub>-4.5</sub>    | 0.18 <sup>+0.09</sup> <sub>-0.07</sub> | 1.00E - 05               | 1.00        |
| GW190701.203306 | 54.1 <sup>+12.6</sup> <sub>-8.0</sub>   | 40.5 <sup>+8.7</sup> <sub>-12.1</sub>  | 90.2 <sup>+11.2</sup> <sub>-8.9</sub>   | 0.38 <sup>+0.11</sup> <sub>-0.12</sub> | 5.70E - 03               | 1.00        |
| GW190706.222641 | 74.0 <sup>+20.1</sup> <sub>-16.9</sub>  | 39.4 <sup>+18.4</sup> <sub>-15.4</sub> | 107.3 <sup>+25.2</sup> <sub>-15.9</sub> | 0.60 <sup>+0.33</sup> <sub>-0.29</sub> | 5.00E - 05               | 1.00        |
| GW190707.093326 | 12.1 <sup>+2.6</sup> <sub>-2.0</sub>    | 7.9 <sup>+1.6</sup> <sub>-1.3</sub>    | 19.2 <sup>+1.7</sup> <sub>-1.2</sub>    | 0.17 <sup>+0.06</sup> <sub>-0.08</sub> | 1.00E - 05               | 1.00        |
| GW190708.232457 | 19.8 <sup>+4.3</sup> <sub>-4.3</sub>    | 11.6 <sup>+3.1</sup> <sub>-2.0</sub>   | 30.1 <sup>+2.9</sup> <sub>-2.1</sub>    | 0.19 <sup>+0.06</sup> <sub>-0.07</sub> | 3.10E - 04               | 1.00        |
| GW190719.215514 | 36.6 <sup>+42.1</sup> <sub>-11.1</sub>  | 19.9 <sup>+10.0</sup> <sub>-9.3</sub>  | 54.5 <sup>+38.3</sup> <sub>-11.1</sub>  | 0.61 <sup>+0.39</sup> <sub>-0.30</sub> | 6.30E - 01               | 0.92        |
| GW190720.000836 | 14.2 <sup>+5.6</sup> <sub>-3.3</sub>    | 7.5 <sup>+2.2</sup> <sub>-1.8</sub>    | 20.8 <sup>+3.9</sup> <sub>-2.0</sub>    | 0.16 <sup>+0.11</sup> <sub>-0.05</sub> | 1.00E - 05               | 1.00        |
| GW190725.174728 | 11.8 <sup>+10.1</sup> <sub>-3.0</sub>   | 6.3 <sup>+2.1</sup> <sub>-2.5</sub>    | 17.6 <sup>+7.7</sup> <sub>-1.8</sub>    | 0.20 <sup>+0.09</sup> <sub>-0.08</sub> | 4.60E - 01               | 0.96        |
| GW190727.060333 | 38.9 <sup>+8.9</sup> <sub>-6.0</sub>    | 30.2 <sup>+6.5</sup> <sub>-8.3</sub>   | 65.4 <sup>+9.5</sup> <sub>-7.3</sub>    | 0.52 <sup>+0.18</sup> <sub>-0.18</sub> | 1.00E - 05               | 1.00        |
| GW190728.064510 | 12.5 <sup>+6.9</sup> <sub>-2.3</sub>    | 8.0 <sup>+1.7</sup> <sub>-2.6</sub>    | 19.7 <sup>+4.4</sup> <sub>-1.4</sub>    | 0.18 <sup>+0.05</sup> <sub>-0.07</sub> | 1.00E - 05               | 1.00        |



Table 1-continued

| Name            | $m_1 (M_\odot)$                         | $m_2 (M_\odot)$                        | $m_f (M_\odot)$                         | redshift                               | FAR(year <sup>-1</sup> ) | $p_{astro}$ |
|-----------------|---|--|---|--|--------------------------|-------------|
| GW190731_140936 | 41.8 <sup>+12.7</sup> <sub>-9.1</sub>   | 29.0 <sup>+10.2</sup> <sub>-9.9</sub>  | 67.4 <sup>+15.3</sup> <sub>-10.8</sub>  | 0.56 <sup>+0.31</sup> <sub>-0.26</sub> | 3.30E - 01               | 0.83        |
| GW190803_022701 | 37.7 <sup>+9.8</sup> <sub>-6.7</sub>    | 27.6 <sup>+7.6</sup> <sub>-8.5</sub>   | 62.1 <sup>+11.2</sup> <sub>-7.6</sub>   | 0.54 <sup>+0.22</sup> <sub>-0.22</sub> | 7.30E - 02               | 0.97        |
| GW190805_211137 | 46.2 <sup>+15.4</sup> <sub>-11.2</sub>  | 30.6 <sup>+11.8</sup> <sub>-11.3</sub> | 72.4 <sup>+18.2</sup> <sub>-13.2</sub>  | 0.92 <sup>+0.43</sup> <sub>-0.40</sub> | 6.30E - 01               | 0.95        |
| GW190828_063405 | 31.9 <sup>+5.4</sup> <sub>-4.1</sub>    | 25.8 <sup>+4.9</sup> <sub>-5.3</sub>   | 54.3 <sup>+7.3</sup> <sub>-4.0</sub>    | 0.38 <sup>+0.10</sup> <sub>-0.15</sub> | 1.00E - 05               | 1.00        |
| GW190828_065509 | 23.7 <sup>+6.8</sup> <sub>-6.7</sub>    | 10.4 <sup>+3.8</sup> <sub>-2.2</sub>   | 33.0 <sup>+5.3</sup> <sub>-4.3</sub>    | 0.29 <sup>+0.11</sup> <sub>-0.11</sub> | 3.50E - 05               | 1.00        |
| GW190910_112807 | 43.8 <sup>+7.6</sup> <sub>-6.8</sub>    | 34.2 <sup>+6.6</sup> <sub>-7.3</sub>   | 74.4 <sup>+8.5</sup> <sub>-8.6</sub>    | 0.29 <sup>+0.17</sup> <sub>-0.11</sub> | 2.90E - 03               | 1.00        |
| GW190915_235702 | 32.6 <sup>+8.8</sup> <sub>-4.9</sub>    | 24.5 <sup>+4.9</sup> <sub>-5.8</sub>   | 54.7 <sup>+6.6</sup> <sub>-5.0</sub>    | 0.32 <sup>+0.11</sup> <sub>-0.11</sub> | 1.00E - 05               | 1.00        |
| GW190916_200658 | 43.8 <sup>+19.9</sup> <sub>-12.6</sub>  | 23.3 <sup>+12.5</sup> <sub>-10.0</sub> | 65.0 <sup>+17.3</sup> <sub>-12.6</sub>  | 0.77 <sup>+0.45</sup> <sub>-0.32</sub> | 2.90E - 03               | 1.00        |
| GW190924_021846 | 8.8 <sup>+4.3</sup> <sub>-1.8</sub>     | 5.1 <sup>+1.2</sup> <sub>-1.5</sub>    | 13.3 <sup>+3.0</sup> <sub>-0.9</sub>    | 0.11 <sup>+0.04</sup> <sub>-0.04</sub> | 1.00E - 05               | 1.00        |
| GW190925_232845 | 20.8 <sup>+6.5</sup> <sub>-2.9</sub>    | 15.5 <sup>+2.5</sup> <sub>-3.6</sub>   | 34.9 <sup>+3.5</sup> <sub>-2.6</sub>    | 0.19 <sup>+0.08</sup> <sub>-0.07</sub> | 7.20E - 03               | 0.99        |
| GW190926_050336 | 41.1 <sup>+20.8</sup> <sub>-12.5</sub>  | 20.4 <sup>+11.4</sup> <sub>-8.2</sub>  | 59.6 <sup>+22.1</sup> <sub>-11.8</sub>  | 0.55 <sup>+0.44</sup> <sub>-0.26</sub> | 1.10E + 00               | 0.54        |
| GW190929_012149 | 66.3 <sup>+21.6</sup> <sub>-16.6</sub>  | 26.8 <sup>+14.7</sup> <sub>-10.6</sub> | 90.3 <sup>+22.3</sup> <sub>-14.6</sub>  | 0.53 <sup>+0.33</sup> <sub>-0.20</sub> | 1.60E - 01               | 0.87        |
| GW190930_133541 | 14.2 <sup>+8.0</sup> <sub>-4.0</sub>    | 6.9 <sup>+2.4</sup> <sub>-2.1</sub>    | 20.2 <sup>+6.1</sup> <sub>-2.0</sub>    | 0.16 <sup>+0.06</sup> <sub>-0.06</sub> | 1.00E - 05               | 1.00        |
| GW191103_012549 | 11.8 <sup>+6.2</sup> <sub>-2.2</sub>    | 7.9 <sup>+1.7</sup> <sub>-2.4</sub>    | 19.0 <sup>+3.8</sup> <sub>-1.7</sub>    | 0.20 <sup>+0.09</sup> <sub>-0.09</sub> | 4.60E - 01               | 0.96        |
| GW191105_143521 | 10.7 <sup>+3.7</sup> <sub>-1.6</sub>    | 7.7 <sup>+1.4</sup> <sub>-1.9</sub>    | 17.6 <sup>+2.1</sup> <sub>-1.2</sub>    | 0.23 <sup>+0.07</sup> <sub>-0.09</sub> | 1.20E - 02               | 0.99        |
| GW191109_010717 | 65.0 <sup>+11.0</sup> <sub>-11.0</sub>  | 47.0 <sup>+15.0</sup> <sub>-13.0</sub> | 107.0 <sup>+18.0</sup> <sub>-15.0</sub> | 0.25 <sup>+0.18</sup> <sub>-0.12</sub> | 1.80E - 04               | 0.99        |
| GW191113_071753 | 29.0 <sup>+12.0</sup> <sub>-14.0</sub>  | 5.9 <sup>+4.4</sup> <sub>-1.3</sub>    | 34.0 <sup>+11.0</sup> <sub>-10.0</sub>  | 0.26 <sup>+0.18</sup> <sub>-0.11</sub> | 2.60E + 01               | 0.68        |
| GW191126_115259 | 12.1 <sup>+5.5</sup> <sub>-2.2</sub>    | 8.3 <sup>+1.9</sup> <sub>-2.4</sub>    | 19.6 <sup>+3.5</sup> <sub>-2.0</sub>    | 0.30 <sup>+0.12</sup> <sub>-0.13</sub> | 1.00E - 05               | 1.00        |
| GW191127_050227 | 53.0 <sup>+47.0</sup> <sub>-20.0</sub>  | 24.0 <sup>+17.0</sup> <sub>-14.0</sub> | 76.0 <sup>+39.0</sup> <sub>-21.0</sub>  | 0.57 <sup>+0.40</sup> <sub>-0.29</sub> | 2.50E - 01               | 0.74        |
| GW191129_134029 | 10.7 <sup>+4.1</sup> <sub>-2.1</sub>    | 6.7 <sup>+1.5</sup> <sub>-1.7</sub>    | 16.8 <sup>+2.5</sup> <sub>-1.2</sub>    | 0.16 <sup>+0.05</sup> <sub>-0.06</sub> | 1.20E - 02               | 0.99        |
| GW191204_110529 | 27.3 <sup>+10.8</sup> <sub>-5.9</sub>   | 19.2 <sup>+5.5</sup> <sub>-6.0</sub>   | 45.0 <sup>+8.7</sup> <sub>-7.5</sub>    | 0.34 <sup>+0.25</sup> <sub>-0.18</sub> | 3.30E + 00               | 0.74        |
| GW191204_171526 | 11.7 <sup>+3.3</sup> <sub>-1.7</sub>    | 8.4 <sup>+1.3</sup> <sub>-1.7</sub>    | 19.2 <sup>+1.7</sup> <sub>-0.9</sub>    | 0.13 <sup>+0.04</sup> <sub>-0.05</sub> | 1.00E - 05               | 0.99        |
| GW191215_223052 | 24.9 <sup>+7.1</sup> <sub>-4.1</sub>    | 18.1 <sup>+3.8</sup> <sub>-4.1</sub>   | 41.4 <sup>+5.1</sup> <sub>-4.1</sub>    | 0.35 <sup>+0.13</sup> <sub>-0.14</sub> | 1.00E - 05               | 0.99        |
| GW191216_213338 | 12.1 <sup>+4.6</sup> <sub>-2.2</sub>    | 7.7 <sup>+1.6</sup> <sub>-1.9</sub>    | 18.9 <sup>+2.8</sup> <sub>-0.9</sub>    | 0.07 <sup>+0.02</sup> <sub>-0.03</sub> | 1.00E - 05               | 1.00        |
| GW191222_033537 | 45.1 <sup>+10.9</sup> <sub>-8.0</sub>   | 34.7 <sup>+9.3</sup> <sub>-10.5</sub>  | 75.5 <sup>+15.3</sup> <sub>-9.9</sub>   | 0.51 <sup>+0.23</sup> <sub>-0.26</sub> | 1.00E - 05               | 0.99        |
| GW191230_180458 | 49.4 <sup>+14.0</sup> <sub>-9.6</sub>   | 37.0 <sup>+11.0</sup> <sub>-12.0</sub> | 82.0 <sup>+17.0</sup> <sub>-11.0</sub>  | 0.69 <sup>+0.26</sup> <sub>-0.27</sub> | 5.00E - 02               | 0.96        |
| GW200112_155838 | 35.6 <sup>+6.7</sup> <sub>-4.5</sub>    | 28.3 <sup>+4.4</sup> <sub>-5.9</sub>   | 60.8 <sup>+5.3</sup> <sub>-4.3</sub>    | 0.24 <sup>+0.07</sup> <sub>-0.08</sub> | 1.00E - 07               | 1.00        |
| GW200128_022011 | 42.2 <sup>+11.6</sup> <sub>-8.1</sub>   | 32.6 <sup>+9.5</sup> <sub>-9.2</sub>   | 71.0 <sup>+16.0</sup> <sub>-11.0</sub>  | 0.56 <sup>+0.28</sup> <sub>-0.28</sub> | 4.30E - 03               | 0.99        |
| GW200129_065458 | 34.5 <sup>+9.9</sup> <sub>-3.1</sub>    | 29.0 <sup>+3.3</sup> <sub>-9.3</sub>   | 60.2 <sup>+4.1</sup> <sub>-3.2</sub>    | 0.18 <sup>+0.05</sup> <sub>-0.07</sub> | 1.00E - 05               | 0.99        |
| GW200202_154313 | 10.1 <sup>+3.5</sup> <sub>-1.4</sub>    | 7.3 <sup>+1.1</sup> <sub>-1.7</sub>    | 16.8 <sup>+1.9</sup> <sub>-0.7</sub>    | 0.09 <sup>+0.03</sup> <sub>-0.03</sub> | 1.00E - 05               | 0.99        |
| GW200208_130117 | 37.7 <sup>+9.3</sup> <sub>-6.2</sub>    | 27.4 <sup>+6.3</sup> <sub>-7.3</sub>   | 62.5 <sup>+7.5</sup> <sub>-6.4</sub>    | 0.40 <sup>+0.15</sup> <sub>-0.14</sub> | 7.30E - 02               | 0.97        |
| GW200208_222617 | 51.0 <sup>+103.0</sup> <sub>-30.0</sub> | 12.3 <sup>+9.2</sup> <sub>-5.5</sub>   | 61.0 <sup>+99.0</sup> <sub>-26.0</sub>  | 0.66 <sup>+0.53</sup> <sub>-0.29</sub> | 4.80E + 00               | 0.70        |
| GW200209_085452 | 35.6 <sup>+10.5</sup> <sub>-6.8</sub>   | 27.1 <sup>+7.8</sup> <sub>-7.8</sub>   | 59.9 <sup>+13.1</sup> <sub>-8.9</sub>   | 0.57 <sup>+0.25</sup> <sub>-0.26</sub> | 1.00E - 07               | 1.00        |
| GW200216_220804 | 51.0 <sup>+22.0</sup> <sub>-13.0</sub>  | 30.0 <sup>+14.0</sup> <sub>-16.0</sub> | 78.0 <sup>+19.0</sup> <sub>-13.0</sub>  | 0.63 <sup>+0.37</sup> <sub>-0.29</sub> | 4.80E + 00               | 0.70        |
| GW200219_094415 | 37.5 <sup>+10.1</sup> <sub>-6.9</sub>   | 27.9 <sup>+7.4</sup> <sub>-8.4</sub>   | 62.2 <sup>+11.7</sup> <sub>-7.8</sub>   | 0.57 <sup>+0.22</sup> <sub>-0.22</sub> | 9.90E - 04               | 0.99        |
| GW200220_061928 | 87.0 <sup>+40.0</sup> <sub>-23.0</sub>  | 61.0 <sup>+26.0</sup> <sub>-25.0</sub> | 141.0 <sup>+51.0</sup> <sub>-31.0</sub> | 0.90 <sup>+0.55</sup> <sub>-0.40</sub> | 6.80E + 00               | 0.62        |
| GW200220_124850 | 38.9 <sup>+14.1</sup> <sub>-8.6</sub>   | 27.9 <sup>+9.2</sup> <sub>-9.0</sub>   | 64.0 <sup>+16.0</sup> <sub>-11.0</sub>  | 0.66 <sup>+0.36</sup> <sub>-0.31</sub> | 1.00E - 05               | 1.00        |
| GW200224_222234 | 40.0 <sup>+6.7</sup> <sub>-4.5</sub>    | 32.7 <sup>+4.8</sup> <sub>-7.2</sub>   | 68.7 <sup>+6.7</sup> <sub>-4.8</sub>    | 0.32 <sup>+0.08</sup> <sub>-0.11</sub> | 1.00E - 05               | 0.99        |
| GW200225_060421 | 19.3 <sup>+5.0</sup> <sub>-3.0</sub>    | 14.0 <sup>+2.8</sup> <sub>-3.5</sub>   | 32.1 <sup>+3.5</sup> <sub>-2.8</sub>    | 0.22 <sup>+0.09</sup> <sub>-0.10</sub> | 1.10E - 05               | 0.99        |
| GW200302_015811 | 37.8 <sup>+8.7</sup> <sub>-8.5</sub>    | 20.0 <sup>+8.1</sup> <sub>-5.7</sub>   | 55.5 <sup>+8.9</sup> <sub>-6.6</sub>    | 0.28 <sup>+0.16</sup> <sub>-0.12</sub> | 1.10E - 01               | 0.91        |

**Table 1-continued**

| Name            | $m_1 (M_\odot)$         | $m_2 (M_\odot)$        | $m_f (M_\odot)$         | redshift               | FAR(year <sup>-1</sup> ) | $p_{astro}$ |
|-----------------|-------------------------|------------------------|-------------------------|------------------------|--------------------------|-------------|
| GW200306_093714 | $28.3^{+17.1}_{-7.7}$   | $14.8^{+6.5}_{-6.4}$   | $41.7^{+12.3}_{-6.9}$   | $0.38^{+0.24}_{-0.18}$ | $2.40E + 01$             | 0.81        |
| GW200308_173609 | $60.0^{+166.0}_{-29.0}$ | $24.0^{+36.0}_{-13.0}$ | $88.0^{+169.0}_{-47.0}$ | $1.04^{+1.47}_{-0.57}$ | $2.40E + 00$             | 0.86        |
| GW200311_115853 | $34.2^{+6.4}_{-3.8}$    | $27.7^{+4.1}_{-5.9}$   | $59.0^{+4.8}_{-3.9}$    | $0.23^{+0.05}_{-0.07}$ | $1.00E - 05$             | 0.99        |
| GW200316_215756 | $13.1^{+10.2}_{-2.9}$   | $7.8^{+2.0}_{-2.9}$    | $20.2^{+7.4}_{-1.9}$    | $0.22^{+0.08}_{-0.08}$ | $1.00E - 05$             | 0.99        |
| GW200322_091133 | $38.0^{+130.0}_{-22.0}$ | $11.3^{+24.3}_{-6.0}$  | $48.0^{+132.0}_{-22.0}$ | $0.59^{+1.43}_{-0.32}$ | $1.40E + 02$             | 0.62        |

Note. The data are taken from the GWTC catalogue (<https://gwosc.org/>). Column 1 represents the name of the GW events. Columns 2, 3 and 4 represent the source masses of the heavier, lighter and remnant object of the mergers. The redshift is listed in Column 5. Columns 6 and 7 represent the false alarm rate (FAR) and the corresponding probability of being astrophysical origin.